Time Delay Calculation of Stress Waves Using Wavelet Analysis Application in Canine Edematous Lungs

Mehran Jahed*, Bizhan Najafi*, Ali Khamene*, and Stephen J. Lai-Fook**

*Department of Electrical Engineering, Sharif University of Tech., Tehran, Iran

**Department of Biomedical Engineering, University of Kentucky, Lexington, KY

ABSTRACT

We examined the relationship between stress wave velocities and the lung density. The discrete cubic spline wavelet was used to calculate time delay and frequency character of the wave that is propagated on the surface of 3 canine lungs. The analysis verified previous results ascertaining the linear elastic model. As vascular volume, extra vascular lung water and lung density increased, wave velocities were decreased; that is wave velocities were inversely proportional to the square root of the lung density. The analysis verified the exact time-frequency relationship for the dominant stress wave velocity (i.e. shear or Rayleigh-Type Surface wave velocity) and showed other transit times besides the previously observed short and long ones are not valid.

1. INTRODUCTION

Vibration and stress wave analysis can be used to characterize lung parenchyma by evaluating elastic constants at various pressure-volume conditions [1,2,3]. In the theory of the stress wave propagation in an elastic continuum, wave velocities are proportional to the square root of the material stiffness, as defined by elastic moduli, and are inversely proportional to the square root of the material density [4]. In this study we examined the behavior of the elastic wave propagation under conditions of increasing lung density at a constant Ptp of 5 cm of water. Transmitted stress waves were analyzed by the discrete wavelet analysis [5,6].

The discrete wavelet transform that was implemented in this study utilized a multi-resolution analysis in the frequency domain. Wavelet and spectral analyses were used to distinguish various types of distorting transient vibrations and associated stress wave propagation modes, measured on the lung. Utilizing the cubic spline wavelet analysis, dominant stress wave velocities were localized and distinguished from other modes of propagation [7].

2. THEORETICAL BACKGROUND

To improve the relation between the time and frequency resolutions [8, 9, 10], Morlet and Grossmann [11] introduced a new method using basic functions, called wavelets, which are dependent on the time shift and dilation of a unique basic function. An example of a basic function is given in Figure 1 for various dilation factors. Each of these functions have similar basic shapes and cyclic variations. Such functions may be suitable to identify signals that hold their character in whole, though suffer nonlinear or Doppler effect variation in their frequency.

Given the wavelet basic function (i.e. mother wavelet), $\Psi(x)$, other basic functions are expressed as,

$$\Psi_{a,\tau}(t) = \frac{1}{\sqrt{a}}\Psi\left(\frac{(t-\tau)}{a}\right) \qquad (1)$$

Figure 1: Basis function of wavelet with different dilation.

where τ is the time shift, a is the dilation factor, and $\sqrt{a}$ is used to normalize the coefficients. Using this definition, its Fourier Transform is given in (2),

$$\Psi_{a,\tau}(f) = \frac{1}{\sqrt{a}} e^{-2\pi i f\tau}\Psi(af) \quad . \qquad (2)$$

Therefore the time-frequency domain may be divided into flexible sized cells suitable for the bandwidth of an appropriate section of the wavelet. That is to say that shorter wavelets (smaller 'a') have wider band in higher frequencies and conversely, longer wavelets (larger 'a') have narrower band in lower frequencies, or

$$C_{a,\tau}(t) = \frac{1}{\sqrt{a}}\int_{-\infty}^{+\infty} x(t)h^*\left(\frac{(t-\tau)}{a}\right)dt \qquad (3)$$

where squared values, $C_{a,\tau}$ represents partial energy of the signal x(t) about time τ and frequency bandwidth proportional to 'a' [9, 10, 12].

Multi-resolution Transform

A multi-resolution transform approximates the signal with different resolutions. Assuming that the resolution of a continuous signal is infinite, then as the number of samples in a desired interval are decreased, the resolution is reduced. If the 'A' operator is defined to approximate the signal under various resolutions, it must be linear, and the approximation of the function with resolution 2^j must be the same as 2^j of the signal. Furthermore among all the approximations f(x), which have similar resolution 2^j, $A_{2^j}f(x)$ must be closest to f(x). Also, if V_{2^j} is the vector space of all the approximated signals

with a resolution of 2^j, then the vector space of V_{2^j} must be a sub-space of $V_{2^{j+1}}$. Lastly, when the function is approximated with the resolution 2^j, as the information on f(x) is partially reduced, with an increase of the resolution to $+\infty$, the approximation must converge to the original signal. Therefore the effect of using the operator, A_{2^j} is to project the original signal to the orthonormal basis of V_{2^j} space.

Mallat [7] showed that the orthonormal basis of the approximated vector space is obtained from the scale and shift of the special function $\Phi(x)$. Consequently, multi-resolution transform operator is found from ,

$$A^d_{2^j} f(x) = \sum_{-\infty}^{+\infty} \frac{< f(u), \phi_{2^j}(u - 2^{-j}n) >}{2^j} . \phi_{2^j}(x - 2^{-j}n) \quad (4)$$

where $\Phi(x)$ is a low pass filter and the operator enclosed by < . >, represents the inner product. The $A_{2^j} f(x)$ which gives the approximation of the f(x) with 2^j resolution, may be represented also with the aid of a discrete group of inner products, $A^d{}_{2^j} f(x)$, as shown below

$$A^f_{2^j} f(n) = \left(\left\langle f(u), \phi_{2^j}\left(u - 2^{-j}n\right) \right\rangle \right)_{n \in z} \quad (5)$$

The $A^d{}_{2^j} f(x)$ is the discrete approximation of f(x) with 2^j resolution, and is therefore more suitable for algorithmic construction on digital computers [7].

According to the mentioned properties of $A^d{}_{2^j}$, it can be shown that using the low-pass filter H(ω), and high-pass filter G(ω), projections of f(x) on the V_{2^j} and O_{2^j} (orthogonal on V_{2^j} space) may be obtained from the projections on $V_{2^{j+1}}$ space. The functions h(n) and g(n) are found as follows, [7] :

$$\left\langle f(u), \phi_{2^j}\left(u - 2^{-j}n\right) \right\rangle = \sum_{k=-\infty}^{+\infty} \tilde{h}(2n-k) . \left\langle f(u), \phi_{2^{j+1}}(u - 2^{-j-1}k) \right\rangle \quad (6)$$

where,

$$h(n) = \left\langle \phi_{2^{-1}}(u), \phi(u-n) \right\rangle \quad (7)$$

$$\tilde{h}(n) = h(-n) \quad (8)$$

and,

$$\left\langle f(u), \varphi_{2^j}\left(u - 2^{-j}n\right) \right\rangle = \sum_{k=-\infty}^{+\infty} \tilde{g}(2n-k) . \left\langle f(u), \varphi_{2^{j+1}}(u - 2^{-j-1}k) \right\rangle \quad (9)$$

where,

$$g(n) = \left\langle \varphi_{2^{-1}}(u), \varphi(u-n) \right\rangle \quad (10)$$

$$\tilde{g}(n) = g(-n) \quad (11)$$

Note that $\varphi_{2^j}(u - 2^{-j}n)_{n \in z}$ are orthonormal functions for the O_{2^j} space. Hence by defining filters, $\tilde{h}$ and $\tilde{g}$, one can derive the approximated 'f' with resolution 2^j from the approximated 'f' with resolution 2^{j+1} and obtain the information in these approximations, namely $D_2{}^j$ f. This method is depicted in Figure 2.

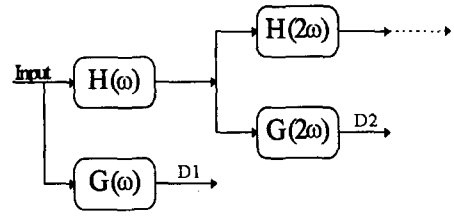

Figure 2: Block diagram of discrete wavelet Algoritms.

3. METHODS

Propagation of stress waves were studied on isolated edematous canine lobes at Ptp of 5 cm of water. An impulse distortion was applied via a solenoid source, and measured with source and receiver miniature microphones [3]. Data was stored on a PC and post processed with PC Matlab.

To study the effect of vascular volume and edema, saline was infused in steps, into the excised and inflated canine lung's vessels. At each step, the transmitted signals at 2 and 7 cm from an impulse surface distortion source were measured with microphones placed on the lung surface [3]. At the beginning and the end of the experiment, a control run without saline in the vasculature was performed (i.e. UNP 1 and 2) [3].

In this analysis, the down sampling procedure was not implemented, since to calculate the time delay, the highest resolution is desired. This action is performed according to the diagram shown in Figure 2 . First to implement this algorithm, appropriate filters, namely H(ω) and G(ω) were designed. These filters had to be designed to distinguish various bands of frequencies, depicting major stress wave propagation frequency bandwidths [2].

For this reason various packs of wavelets were implemented including the Daub4, Haar, Daub20, cubic spline, and the quadratic spline [5,6,7,8,9]. The cubic spline, resulted in the best resolution in frequency and time domains, given its orthonormal character. Such advantage is however overshadowed by the fact that this wavelet is not compactly supported and hence the computation complexity was relatively intense.

The cubic spline methods may be represented in terms of scaling function choices, where it is arranged as a spline of 2p+1 degree as shown below,

$$\phi(\omega) = \frac{1}{\omega^n \sqrt{\sum_{2n}(\omega)}} \quad . \quad (12)$$

In this equation, n=2+2p and the function $\Sigma_{2n}(\omega)$ is defined using Eq (13) [7],

$$\sum_{2n}(\omega) = \sum_{k=-\infty}^{+\infty} \frac{1}{(\omega + 2k\pi)^n} \quad . \quad (13)$$

Using this definition, H(ω) and G(ω) may be calculated using the functions,

$$H(\omega) = \sqrt{\frac{\sum_{2n}(\omega)}{2^{2n} \sum_{2n}(\omega)}} \quad (14)$$

$$G(\omega) = e^{-j\omega} H(\omega + \pi) \qquad (15)$$

where the cubic spline is obtained for p=1, or n=4.

As the sampling frequency for the gathered signals is 2KHz, using the values given in Table 1 to separate various modes of wave propagation on the lung surface, a 2^5 scale with a frequency limit of 43-82 Hz is utilized. Therefore the input (source) and output (receiver or destination) signals are analyzed in fifth scale and their peaks are compared. The time difference between these peaks is chosen as the time delay of interest. Given the distance between the source and destination microphones, stress wave velocity is calculated through the following relations [1,2,3],

$$V = \frac{d}{T_{delay}} \quad \text{(cm/s)} \qquad (16)$$

$$\rho_i = \frac{V^2}{\mu} \quad \text{(g/cm}^3\text{)} \qquad (17)$$

TABLE 1

SCALE	C.O.F H(ω)	C.O.F G(ω)
1.	**1.0278**	**2.114 - 4.169**
2.	**0.5123**	**1.080 - 2.083**
3.	**0.2546**	**0.531 - 1.040**
4.	**0.1258**	**0.267 - 0.519**
5.	**0.0614**	**0.135 - 0.258**
6.	**0.0307**	**0.068 - 0.129**

4. RESULTS and ANALYSIS

Figure 4 shows output signals from the wavelet transform of the source and destination microphone signals with a scaling factor of 2^5. The clean and visible time delay between these signals is an interesting outcome of this technique. In Figure 5a the frequency spectrum of the source signal with (2^5 scale) and without the application of the wavelet transform is shown. Figure 5b depicts a similar pattern for the destination signal. These figures verify the validity of the usage of the 2^5 scale for this analysis.

Figure 6 shows the outputs of the wavelet transform for the destination signal for various scaling in time domain. Figure 7 (the contour plot) shows the frequency spectrum for the same signal for the same scaling. As seen from these Figures, in terms of time and frequency representations, the maximum signal exists in forth and fifth scales, that is in the range of 45 to 165 Hz. Moreover, the ultimate peak in time domain and in the power spectrum belongs to the fifth scale or 2^5.

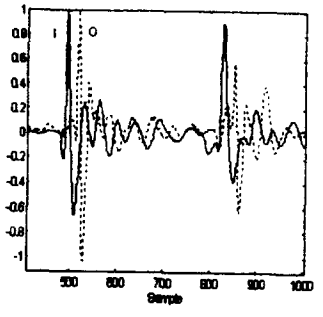

Figure 4: Output signal from the wavelet transform of the source and destination signals.

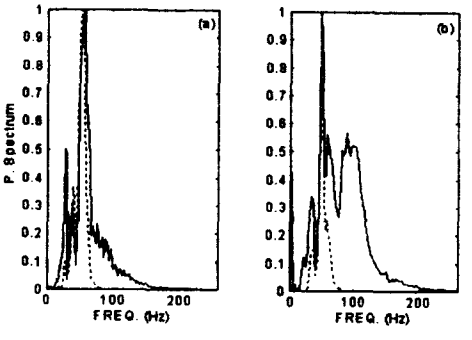

Figure 5: (a) Power spectrum of the source signal using the fifhs scale (dash line) and without the application of wavelet (solid line) (b) similar pattern for the destination signal.

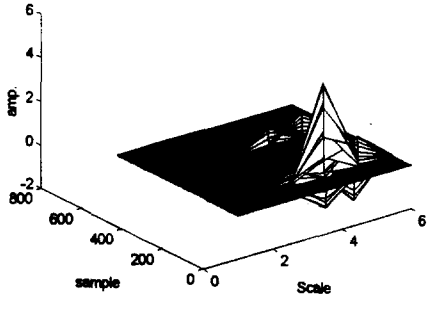

Figure 6: Outputs of the wavelet transform for the destination signal for various scales in the time domain.

These results suggest that the velocity of the propagated waves on the surface of the canine lungs resemble both the shear or Rayleigh-Type Surface wave (as the most dominant wave), and the longitudinal wave velocities. Other modes of propagation are extremely weak.

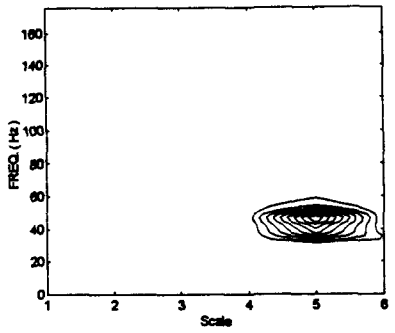

Figure 7: Contour graph on scale-frequency plane.

To further study the dominant propagated stress wave, the results from the 2^5 scale were compared to the theoretical stress wave velocities based on the elastic moduli estimation values. Table 2 depicts velocity and density, ρ_i , calculated from equations, (16) and (17), and also ρ_v , which is the calculated density based on the amount of water infused into the lungs and the estimated shear modulus [1].

TABLE 2

	UP 1	P1	P2	P3	P4	P5	P6	P7	2
V	128	105	98	93	86	83	78	74	80
pi	.15	.21	.27	.3	.4	.45	.5	.7	.6
pv	.22	.33	.38	.4	.5	.52	.6	.7	.6

These results suggest that as the water accumulation in the vasculature or lung density is increased, the velocity of the stress wave is decreased, as predicted from Eq. (17). For the final unperfusion control test, after an irreversible water accumulation has occurred in the lung, it seems that due to the vasculature trap, water is not ejected out of the lung completely in the region of stress wave measurement and the velocity of the stress wave may not match that of the theoretical density change (Table 2).

Figure 8 shows the stress wave velocities for various densities for all three canine lungs tested. A second degree polynomial was fitted to this data. The curve fit is calculated based on the theoretical stress wave velocities.

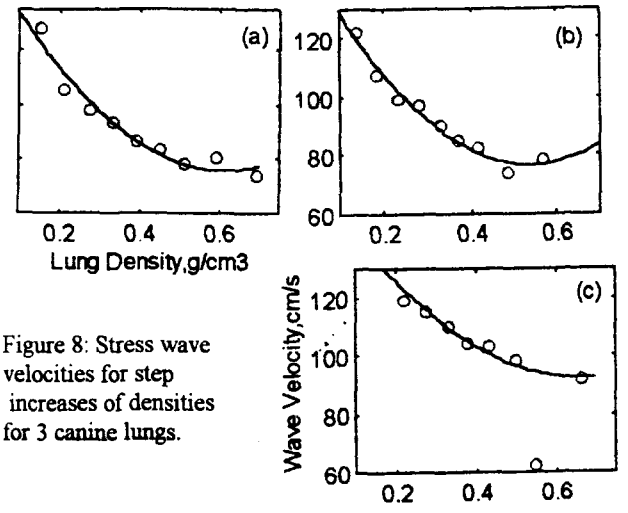

Figure 8: Stress wave velocities for step increases of densities for 3 canine lungs.

5. CONCLUSION

The output of the energy localization algorithm was an accurate measure of time delay of the source and receiver signals, placed at 2 and 7 cm away from the impulse distortion source. Stress wave velocities calculated from the transit time were compared to a theoretical estimate which is based on the linear elastic model of the lung as a homogeneous and isotropic material. The results verified our previous findings [3] and gave evidence of the exact energy localization regions.

Using the mentioned wavelet transform, we were able to separate Rayleigh-Type Surface wave velocity (or shear) from other types of waves. This analysis, enabled us to measure the amount of edema in canine excised lungs and minimize the amount of interference of other waves.

6. REFERENCES

[1] S. J. Lai-Fook, T. A. Wilson, R. E. Hyatt, and J. R. Rodarte, "Elastic constants of inflated lobes of dog lungs", Journal of Applied Physiology, vol. 40, pp. 508-513, 1976.

[2] M. Jahed, "An investigation of Stress Wave Propagation in Inflated Isolated Lungs via Digital Signal Analysis", Ph.D. Dissertation, University of Kentucky, 1990.

[3] M. Jahed, S. J. Lai-Fook, and P. K. Bhagat, "Effect of vascular volume and edema on wave propagation in canine lungs", Journal of Applied Physiology, vol. 68(5), pp. 2171-2176, 1991.

[4] H. Kolsky, "Stress Waves in Solids", New York,; Dover, 1963.

[5] I. Daubechies, "Ten Lectures on Wavelets", SIAM, Philadelphia, 1992.

[6] I. Daubechies, "Orthogonal Bases of Compactly Supported Wavelets", Comm. in Pure Appl. Math., vol. 41, 909-996, 1988.

[7] S. Mallat, "A theory for Multi-resolution signal decomposition 'The Wavelet representation' ", IEEE Trans. Pattern Anal & Machine Intelligence, vol. 11(7), 674-693, 1989.

[8] D. Gabor, "Theory of Communication", Journal of IEEE, vol. 93, pp. 429-457, 1946.

[9] O. Rioul and M. Vetterli, "Wavelets and Signal Processing", IEEE SP Mag., pp. 14-38, 1991.

[10] L. G. Weiss, "Wavelets and Wide band Correlation Processing", IEEE Signal Proc. Mag., pp. 13-31, 1994.

[11] A. Grossman and J. Morlet, "The Composition of Hardy Functions into Square Integrable Wavelets of Constant Shape", SIAM J. Math, Vol. 15, pp. 723-736, 1984.

[12] Y. Meyers, "Wavelets Algorithms and Applications", SIAM, 1993.